Regulation of anterior neurectoderm specification and differentiation by BMP signaling in ascidians

Agnès Roure, Rafath Chowdhury, Sébastien Darras

Regulation of anterior neurectoderm specification and differentiation by BMP signaling in ascidians

Agnès ROURE, Rafath CHOWDHURY* and Sébastien DARRAS#

Sorbonne Université, CNRS, Biologie Intégrative des Organismes Marins (BIOM), F-66650, Banyuls/Mer, France

*: present address: Departament de Genètica, Microbiologia i Estadistica, Facultat de Biologia, Universitat de Barcelona, Spain

#: author for correspondence (sebastien.darras@obs-banyuls.fr)

Running title

Palps and BMP in ascidians

Keywords

palps, ascidian, BMP, anterior neural boundary, placode, peripheral nervous system

Summary statement

BMP signaling regulates two steps of ascidian palp formation: presumptive territory specification at the anterior neural plate border during gastrulation, and ventral palp *vs* inter-palp segregation during neurulation.

Abstract

The most anterior structure of the ascidian larva is made of three palps with sensory and adhesive functions essential for metamorphosis. They derive from the anterior neural border and their formation is regulated by FGF and Wnt. Since they also share gene expression profiles with vertebrate anterior neural tissue and cranial placodes, their study should shed light on the emergence of the unique vertebrate telencephalon. We show that BMP signaling regulates two phases of palp formation in *Ciona intestinalis*. During gastrulation, the anterior neural border is specified in a domain of inactive BMP signaling, and activating BMP prevented its formation. During neurulation, BMP defines ventral palp identity and indirectly specifies the inter-papilla territory separating the ventral and dorsal palps. Finally, we showed that BMP has similar functions in the ascidian *Phallusia mammillata* for which we identified novel palp markers. Collectively, we provide a better molecular description of palp formation in ascidians that will be instrumental for comparative studies.

Introduction

Ascidians (or sea squirts) belong to a group of marine invertebrates, the tunicates, that is the sister group of vertebrates (Delsuc et al., 2006). This phylogenetic position associated with a stereotyped embryonic development with few cells puts ascidians as interesting models for developmental biology and comparative approaches to address questions regarding chordates evolution and the emergence of vertebrates. Ascidians have a biphasic life cycle: following external development, the embryo gives rise to a swimming tadpole-like larva with typical chordate features (notochord, dorsal neural tube) that is going to attach to a substrate before metamorphosing into a sessile adult ascidian with a radically different body plan, a 'bag' with two siphons. Metamorphosis is controlled by a specific organ, the palps (also referred to as the adhesive organ or the adhesive papillae), that is located at the anterior end of the larva. The palps are a specialized part of the ectoderm that has adhesive and sensory properties (Cloney, 1977; Imai and Meinertzhagen, 2007; Satoh, 1994). They enable the larva to select a suitable substrate for metamorphosis, hence a chemo- and/or mechano-sensory function, and to attach to it through the secretion of adhesive materials (reviewed in (Pennati and Rothbächer, 2015)). It contains at least four cells types whose specification and function have not yet been deciphered in details (Johnson et al., 2020; Zeng et al., 2019). Three cell types - the ciliated sensory neurons, the collocytes (containing vesicles filled with adhesive material), and the axial columnar cells (ACCs) (myoepithelial cells controlling palp retraction following adhesion) - are elongated cells forming a protrusion. Three protrusions or papillae (two dorsal papillae that are bilaterally symmetrical, and a ventral papilla located at the midline; Fig. 1C) make up the palps and are separated by the fourth cell type, the non-elongated inter-papillae cells.

Palps belong to the peripheral nervous system and have been instrumental for proposing evolutionary scenarios on the nervous system in chordates (Cao et al., 2019; Horie et al., 2018; Poncelet and Shimeld, 2020; Thawani and Groves, 2020). In the ascidian *Ciona intestinalis*, palp cell lineage and topology, together with gene expression data and functional studies, have shown affinities with anterior derivatives of the vertebrate nervous system, the olfactory placodes and the telencephalon (Cao et al., 2019; Horie et al., 2018; Hudson et al., 2003; Liu and Satou, 2019; Poncelet and Shimeld, 2020; Thawani and Groves, 2020; Wagner and Levine, 2012; Wagner et al., 2014). Palps originate from precursors that are located at the anterior edge of the neural plate during gastrulation, that we will refer to

as the anterior neural border (ANB) (Fig. 1W,X) (Horie et al., 2018; Liu and Satou, 2019). While the ANB is not part of the central nervous system (CNS), it originates from the same lineage specified by FGF-mediated neural induction at the 32-cell stage and expresses neural markers such as *Celf3/4/5/6* (also known as *Etr* and *Celf3.a*) and *Otx* (Horie et al., 2018; Hudson, 2016; Hudson et al., 2003; Nishida, 1987). The separation between these two lineages is regulated by FGF/Erk signaling at gastrula/neurula stages, FGF being active in the CNS precursors (Hudson, 2016; Hudson et al., 2003; Wagner and Levine, 2012). FGF signaling thus regulates positively and negatively two separate phases of palp specification. The ANB also expresses *Dmrt* and *Foxc*, coding for transcription factors that are essential for palp formation (Imai et al., 2006; Wagner and Levine, 2012). From neurulation and through differentiation, palps express genes such as *Dlx.c*, *Foxg*, *Isl* or *Sp6/7/8/9* (also known as *Zf220* and *Btd*) whose orthologs specify anterior neural territories and placodes in vertebrates (Cao et al., 2019; Liu and Satou, 2019; Wagner et al., 2014). In particular, *Foxg* and *Isl* are essential for palp formation (Liu and Satou, 2019; Wagner et al., 2014). The ANB thus shares similarities with vertebrate anterior cranial placodes; and the palps share similarities with derivatives of the vertebrate telencephalon such as the olfactory bulb and of the anterior placodes. It has been proposed that co-option of ANB/palp gene network to the anterior CNS led to the emergence of the vertebrate telencephalon (Cao et al., 2019). While knowledge on transcription factors functions and interactions in palp formation has been elucidated in some detail (Horie et al., 2018; Liu and Satou, 2019; Wagner et al., 2014), the role of cell-cell communication is scarce except for the involvement of FGF/Erk pathway (Hudson et al., 2003; Wagner and Levine, 2012). While we have previously shown that inhibition of canonical Wnt pathway is essential for ANB specification (Feinberg et al., 2019), the description of a later function for Wnt signaling is still lacking. In a distantly related ascidian species *Halocynthia roretzi*, morphological data indicate that activating BMP pathway abolishes palp formation while BMP inhibition results in palps made of a single protrusion instead of three (Darras and Nishida, 2001). But the lack of molecular analysis prevents from precisely determining the function of BMP signaling.

We have directly addressed the function of BMP signaling pathway in palp formation during the embryogenesis of the ascidian *C. intestinalis*. We show that BMP is involved in two consecutive phases. Up to neurulation, ANB specification is incompatible with active BMP signaling; and the ANB forms in a region devoid of active BMP (as revealed by phospho-

Smad1/5/8 immunostaining). Consequently, early activation of BMP prevents palp formation through the inhibition of ANB precursors formation. Following gastrulation, BMP participates in the differentiation of the palps through the specification of the ventral papilla and the regulation of the papillae *vs* inter-papillae fate decision. In particular, BMP-inhibited larvae harbor a single large protrusion made of elongated cells, the *Cyrano* phenotype, with an increased number of sensory neurons and ACCs. We propose that the competence to become a papilla is regulated by BMP through the transcription factors coding genes *Foxg* and *Sp6/7/8/9*. Interestingly, we show that modulating BMP pathway in the ascidian *Phallusia mammillata* (275 My of divergence time) produces the same phenotypes as in *C. intestinalis*. This allowed us to use previously published RNA-seq data (Chowdhury et al., 2022) to identify a number of novel genes expressed in the ANB and the palps. Altogether, our work points to a role for signaling pathways inhibition in ANB specification, similarly to early anterior neurectoderm formation in vertebrates. Moreover, we provide a significant enrichment of the palp gene network, an essential requisite to probe its conservation with the networks regulating cranial placodes and telencephalon formation in vertebrates.

Results

BMP activation abolishes palp formation

When we activated the BMP signaling pathway by overexpressing, in the ectoderm, the BMP ligand Admp by electroporation using the pFog driver (active from the 16-cell stage) (Pasini et al., 2006; Rothbacher et al., 2007), we observed an absence of protrusions that are obvious features of the adhesive palps. The anterior end of the larvae were smooth, and epidermal cells were flat and did not display the typical elongated shape (Fig. 1A-D). This morphological evidence was accompanied by the repression of the expression at mid-tailbud stages of all the genes expressed in the palps that we have examined: *Sp6/7/8/9*, *Isl*, *Foxg*, *Celf3/4/5/6*, *Pou4* and *Emx* (Fig. 1E-P). Palps derive from the median anterior neural border (ANB) at gastrula stages (Fig. 1W,X) and can be tracked by the expression of genes essential for palp formation, *Foxg* at neurula stages (Fig. 1Q,R) and *Foxc* at gastrula stages (Fig. 1U,V) (Liu and Satou, 2019; Wagner and Levine, 2012). Both genes were repressed by BMP activation; and this repression is sufficient to explain the later lack of palp gene expression and differentiation. Interestingly, palps were not converted into general epidermis since the epidermal marker *Sox14/15/21* (also known as *SoxB2*) was normally expressed and did not show ectopic expression in the palp area (Fig. 1S,T).

Dynamic BMP activity in the palp forming region

The above results suggest that active BMP signaling is incompatible with palp formation. Active BMP signaling can be determined by examining the phosphorylated (active) form of the BMP transducer Smad1/5/8. It has been previously shown that BMP is active from late gastrula to early tailbud stages in the ventral epidermis midline of *C. robusta* embryos (Waki et al., 2015). We obtained similar results in *C. intestinalis* using a different antibody (Fig. 2). More specifically, up to gastrulation, we did not detect significant levels for P-Smad1/5/8 except in a few posterior endomesodermal cells (Fig. 2A). At mid-gastrula, P-Smad1/5/8 was present in the nuclei of the posterior (b-line) ventral midline epidermis (Fig. 2B). Consequently, at the onset of *Foxc* expression in palp precursors (St. 10), BMP is not active in the palp forming region (Fig. 2L). Shortly later, at early neurula stages, P-Smad1/5/8 extended into the anterior (a-line) ventral midline epidermis (Fig. 2C). During neurulation, the posterior limit of P-Smad1/5/8 gradually shifted anteriorly in agreement with the

dynamic posterior to anterior expression of candidate target genes (Roure and Darras, 2016); by mid-tailbud stages, P-Smad1/5/8 was restricted to the trunk ventral epidermis (Fig. 2D,E,J). In addition, active Smad1/5/8 was also detected in the endoderm underlying the ventral epidermis midline with a similar temporal dynamic (Fig. 2E,F,H,J,K), and in a group of cells of the anterior sensory vesicle at mid-tailbud stages (Fig. 2E,J,K). We validated the specificity of these results by modulating BMP pathway: when embryos were treated with BMP2 protein, P-Smad1/5/8 was ectopically detected in the entire epidermis at early neurula stages, while no staining was observed following inhibition using the pharmacological inhibitor DMH1 (Fig. S1).

To precisely relate the location of active signaling in the ectoderm and palp precursors, we performed double staining: P-Smad1/5/8 and *in situ* hybridization for the early palp markers *Foxc* and *Foxg* (Fig. 2F-J). At late gastrula stages, P-Smad1/5/8 abutted *Foxc* expression domain, confirming that palp precursors were specified in a BMP-negative domain (Fig. 2F,G,L). Later, we observed P-Smad1/5/8 in the median *Foxc* expression domain at mid neurula stages (not shown) and in the median part of the U-shaped *Foxg* expression domain in late neurulae (Fig. 2H,I,L), corresponding presumably to the future ventral palp. This was confirmed by co-expression of P-Smad1/5/8 and *Foxg* in ventral cells of early tailbuds (Fig. 2J,K,L). In summary (Fig. 2K-L), BMP signaling is absent from the ANB marked by *Foxc* until the early neurula stages; active BMP signaling is detected from mid neurula stages in the future protrusion (*Foxg*$^{+}$ cells) of the ventral palp.

BMP inhibition participates in ANB definition

We next tested whether BMP inhibition was sufficient to induce an ANB fate. When BMP signaling was blocked either by overexpression of the secreted inhibitor Noggin or by treatment with the BMP receptor inhibitor DMH1, *Foxc* expression at late gastrula stages was unchanged (Fig. 3A-C). The fact that *Foxc* was not ectopically expressed following BMP inhibition could be explained by an incomplete BMP blockade. However, DMH1 treatment led to undetectable P-Smad1/5/8 levels (Fig. S1). Alternatively, it could be that the number of cells that are competent to become ANB in response to BMP inhibition could be restricted to the cells already expressing *Foxc*. *Foxc* expression and palp fate are regulated by FGF signaling following neural induction and cell fate segregation (Wagner and Levine, 2012). We thus aimed at increasing the number of cells competent to form ANB by early activation of

FGF signaling using treatment with recombinant bFGF protein, and testing the effects of BMP pathway modulations in this context. As expected, bFGF treatment from the 8-cell stage neuralized the entire ectoderm as revealed by the ectopic expression of the neural markers *Otx* and *Celf3/4/5/6* and the downregulation of the epidermal marker *Tfap2-r.b* (also known as *Ap2-like2*) at late gastrula stages (Fig. 3iv). *Foxc* behaved somewhat unexpectedly: it was either ectopically expressed in a fraction of the embryos (53%, n=69; Fig. 3Giv) or repressed in the others (38%, n=69; not shown). The repression of *Foxc* might be explained by the fact that FGF/Erk is downregulated in the palp lineage during gastrulation (Wagner and Levine, 2012), hence our continuous treatment might inhibit *Foxc* expression. Nevertheless, when BMP pathway was inhibited on top of FGF activation, *Foxc* was strongly expressed, in all embryos, as a cup covering the anterior end including the ventral epidermis (Fig. 3Gvi). Our observations demonstrate that *Foxc* expression and ANB formation can only occur in a domain devoid of active BMP signaling.

Importantly, the loss of *Foxc* following BMP activation using recombinant BMP2 protein treatment was specific to this gene and did not result from neural tissue inhibition as in vertebrates since the neural markers *Otx* and *Celf3/4/5/6* were still expressed in the CNS but downregulated in the ANB (Fig. 3ii). Reciprocally, BMP inhibition was not sufficient to lead to ectopic neural tissue formation (Fig. 3iii). This is in agreement with similar data produced in the distantly related ascidian *Halocynthia roretzi* (Darras and Nishida, 2001). Interestingly, while *Foxc* and *Tfap2-r.b* were co-expressed in the ANB, only *Foxc* was repressed by BMP (Fig. S2). However, since the ANB does not convert into epidermis (Fig. 1), it is likely that, while inhibiting palp fate, BMP signaling does not abolish all the effects of the induction by FGF.

The BMP signaling pathway regulates palp formation after ANB is specified

We examined whether modulating BMP had any impact on palp formation besides ANB specification. We thus performed whole embryo treatments starting at progressively later stages of embryonic development and examined the early marker *Foxc* and the late marker *Isl* (Fig. 4).

Activating BMP at early gastrula stages (St. 10) partially repressed *Foxc* while mid-gastrula (St. 12) treatment had no effect. The time-dependent effects of BMP activation coincide with the dynamics of *Foxc* expression: before it was expressed (8-cell stage), the repression was complete (Fig. 3Gii); at the onset of expression (St. 10), the repression was milder; and

once *Foxc* was robustly expressed (St. 12), there was no repression. This is further supported by the fact that BMP2 treatment led to fast P-Smad1/5/8 nuclear accumulation (the shortest treatment we have tested is 30 min; Fig. S1). The ventral spot of *Isl* expression was lost for treatments starting at St. 10 and St. 12, while later treatments did not change *Isl* expression. Inhibiting BMP had no effect on *Foxc* expression similarly to the earliest treatment (Fig. 3Giii). *Isl*, that is normally expressed as 3 spots, had a U-shaped expression. The same effect was observed by overexpressing Noggin using electroporation (Fig. S3). This phenotype was much less frequent when the DMH1 treatment started at late neurula stages (St. 16).
The changes in *Isl* expression prompted us to determine how palps differentiate when BMP is modulated from gastrula stages.

A single protrusion with additional neurons following BMP inhibition

In DMH1-treated embryos, while *Isl* was expressed following a large U at mid-tailbud stages (St. 23) (Fig. 4), it was concentrated in a protruding structure at the anterior tip at late tailbud stages (St. 25) (Fig. 5E). In larvae, this single large protrusion was made of elongated cells as visualized by phalloidin staining (Fig. 5F-H). We coined this phenotype *Cyrano* (in memory of the famous character depicted by Edmond Rostand). In *Ciona*, it is thought that palps contain a fixed number of the different cell types (Zeng et al., 2019). We performed fluorescent *in situ* hybridization at late-tailbud stages (St. 23) using four genes and made 3D reconstruction of the z-stacks acquired by confocal microscopy (see Material and Methods) in order to determine the differentiation of the palps in the *Cyrano* embryos. In agreement with previous reports, we found that the ACC marker *Isl* was expressed in 12 cells in control embryos (4 cells par papilla) (Fig. 5I-J,Q). By contrast, we found that the sensory neuron marker *Pou4* was expressed in 10 cells instead of 12 (Fig. 5I-J,Q). Interestingly, both dorsal palps had four cells that surrounded the *Isl*-positive cells while the ventral palp contained two *Pou4*-positive cells located dorsally to the *Isl*-positive cells. In DMH1-treated embryos, the number of neurons increased to 18 on average and the number of ACCs to 18 (Fig. 5Q). The increase of *CeIf3/4/5/6* cells was not statistically significant. Interestingly, the number of cells expressing *Sp6/7/8/9*, that has been described as an inter-papillae marker (Wagner et al., 2014), was decreased in DMH1-treated embryos (Fig. 5Q). These data are in agreement with the interpretation that the number of cells with papilla fate has increased, however their physical proximity likely leads to the formation of a single protrusion.

In DMH1 embryos, *Pou4* was expressed all around the *Isl* cells like in the dorsal palps (Fig. 5M,N). This suggested that the *Cyrano* protrusion may have a dorsal identity. In support of this interpretation, we found that the expression of the homeobox transcription factor *Msx*, that we found transiently expressed in the future ventral palp at the onset of *Isl* expression (Fig. 5K,L), was lost following BMP inhibition (Fig. 5O,P). While we have performed a detailed analysis of the *Cyrano* phenotype only on embryos generated by DMH1 treatment starting at gastrula stages, a similar phenotype was observed upon Noggin overexpression (a single protrusion visualized by phalloidin staining in Fig. 5F; U-shape/ectopic expression of *Isl* and *Celf3/4/5/6* in Fig. S3). In *Cyrano* embryos, the ventral palp is missing, the number of inter-palp cells is reduced, and there is an excess of dorsal protruding cells. This suggests that BMP is required to specify the ventral palp and inter-palp cells. When this pathway was inhibited, cells that have lost these fates would adopt a 'default' dorsal palp fate.

The ventral palp is missing following BMP activation

As expected from the *Isl* profile (Fig. 4), only 2 protruding papillae made of elongated cells developed dorsally in BMP2 treated embryos (Fig. 6G,H). This morphological absence of ventral palp was only partially confirmed at the molecular level. Similarly to *Isl*, *Msx* expression was abolished in treated embryos, but the expression of *Pou4* revealed that one or two neurons were still present (Fig. 6I,J). *Sp6/7/8/9* was repressed in its most ventral expression domain (Fig. 6K). In conclusion, while the ventral protrusion is absent, palp identity is not completely suppressed. Accordingly, we did not detect ectopic expression of the epidermal gene *Sox14/15/21* (Fig. 6L).

While BMP is required to define ventral palp fate (Fig. 5), BMP activation does not lead to ectopic ventral palp formation nor ventralizes the dorsal palps (we did not detect obvious defects in dorsal palp differentiation, and identified 4 $Pou4^{+}$ cells surrounding Isl^{+} cells as in controls, Fig. 6I). Since BMP suppresses ventral palp, it is likely that excessive or precocious BMP signaling levels are responsible for this phenotype.

BMP controls ventral palp and inter-palp fates through *Sp6/7/8/9* regulation

The U-shape pattern of *Isl* in DMH1 embryos reminded us of endogenous *Foxg* expression (Liu and Satou, 2019): at neurula stages, *Foxg* was expressed in the future palps following a U-shape that gradually converted into a 3-spots pattern at tailbud stages that prefigures the

three papillae protrusions (Fig. 7A-D). It thus seems that inhibiting BMP prevented the refinement of *Foxg* expression. Accordingly, *Foxg* expression was U-shaped following DMH1 treatment (Fig. 7E). Interestingly, knockdown of the zinc finger transcription factor coding gene *Sp6/7/8/9* leads to a U-shaped *Foxg* expression (Liu and Satou, 2019). Since *Sp6/7/8/9* and *Foxg* are initially partially co-expressed before showing exclusive patterns (Fig. 2L), it has been proposed that *Foxg* restriction to the future protrusions is the result of repression by Sp6/7/8/9. We thus determined *Sp6/7/8/9* and *Foxg* expression following BMP modulation from early gastrula stages (Fig. 7). While we have confirmed initial co-expression using double fluorescent *in situ* hybridization, we have failed to get robust simultaneous expression allowing analysis the effects of the treatments (not shown). At St. 15/16, this is the onset of *Sp6/7/8/9* expression and it was barely detectable (Fig. 7F), and at St. 18/19 when *Sp6/7/8/9* expression was strong, *Foxg* showed a transient downregulation (Fig. 7B). We thus analyzed each gene at different stages (*Foxg* at late neurula stages (St. 16) and *Sp6/7/8/9* at initial tailbud stages (St. 18)). When embryos were treated with BMP2 protein, the ventral expression of *Foxg* in the U-shape was missing (Fig 7J) and *Sp6/7/8/9* was ectopically expressed at this location (Fig. 7M). Reciprocally, following DMH1 treatment, *Foxg* was unchanged (Fig. 7K) and ventral *Sp6/7/8/9* expression was shifted to a median position (Fig. 7N). Hence, *Sp6/7/8/9* was no more expressed in the ventral part of the U-shaped palp forming row of cells (Fig 7T). We summarized our understanding of these results on schematic embryos (Fig. 7O-T). Interestingly, DMH1 treatment had limited effects on *Isl* expression at St. 16 (Fig. 4), a timing that coincides with the onset of *Sp6/7/8/9* expression (Figs 2N,7F).

Our results indicate that *Sp6/7/8/9* is positively regulated by BMP signaling. However, since it is not expressed in P-Smad1/5/8^{+} cells (Fig. 2L), we propose that an intermediate, yet unidentified, factor activates *Sp6/7/8/9* downstream of BMP in the neighboring cells (Fig. 7U,V). This hypothetical model of gene interaction is sufficient to explain *Sp6/7/8/9* and *Foxg* expression patterns and final phenotypes (Fig. 7U-X). Importantly, our data show that dorsal-most cells of the *Foxg* U-shape and dorsal palps develop independently of BMP signaling. In conclusion, we propose that the ventral papilla and the papilla *vs* inter-papilla fate choice is controlled by BMP signaling through the indirect regulation of *Sp6/7/8/9* expression.

Palp formation is similarly regulated by BMP in *P. mammillata*

We aimed at determining the conservation of the role of BMP in palp formation by examining embryos of the ascidian *P. mammillata* that belongs to the same family as *Ciona*, the Phlebobranchia, but with a significant divergence time (275 My) (Fig. 8A) (Delsuc et al., 2018). First, we determined that BMP signaling was active is the ventral part of the embryo with a similar dynamic to *Ciona* as revealed by P-Smad1/5/8 immunostaining (Fig. S4). Next, we identified single orthologs for *Celf3/4/5/6*, *Pou4* and *Isl* genes, that were all expressed in the palps (Fig. 8) (Chowdhury et al., 2022; Coulcher et al., 2020; Dardaillon et al., 2020). Treatment with recombinant BMP2 protein from the 8-cell stage abolished expression of all three markers in the palps, like in *Ciona* (Fig. 8). Following DMH1 treatment from the 8-cell stage, both *Celf3/4/5/6* and *Isl* were expressed in the palp territory following a U-shape pattern like in *Ciona* but not in all cases. For a large fraction of embryos, the pattern appeared as two bars of intense staining resembling the U-shape but without the ventral part. This phenotype that we did not observe in *Ciona* might reveal some differences in the role of BMP in the two species.

Given the overall similar effects on palp formation after alterations of BMP signaling, we sought to identify novel palp molecular markers by using a dataset previously generated in *P. mammillata* (Chowdhury et al., 2022). We had generated, at several developmental stages, RNA-seq data for whole embryos treated with recombinant BMP4 protein and/or DAPT, a pharmacological Notch inhibitor. We identified 1098 genes repressed by BMP signaling at least at one developmental stage (Table S1). In this list, we found the orthologs for 11 well defined *Ciona* palp markers; and 4 of them (*Otx*, *Isl*, *Atoh1/7* and *Celf3/4/5/6*) were described as expressed in the palp lineage in *Phallusia* (Coulcher et al., 2020; Dardaillon et al., 2020). Using Gene Ontology analysis, we selected a list of 53 genes encoding developmental regulators (transcription factors and signaling molecules) or involved in neural tissue formation, and examined their expression patterns (Table S2). Within this list, the expression patterns of 26 genes were previously determined (from the Aniseed database (Dardaillon et al., 2020) and from our previous data (Chowdhury et al., 2022; Coulcher et al., 2020)); and 12 of them were expressed in the palps. We performed *in situ* hybridization for the remaining 27 genes, and discovered 7 novel palp markers whose expression is shown in Fig. 9.

Surprisingly, by examining the expression data generated previously, we found that some genes with palp expression were up-regulated by BMP in our dataset, such as *Chrdl* and *Nos* (Table S2 and Fig. 9A,K). To have a broader view of the potential effect of BMP signaling on gene regulation in the palps, we gathered, from previous publications (Chen et al., 2011; Chowdhury et al., 2022; Coulcher et al., 2020; Joyce Tang et al., 2013; Kusakabe et al., 2012; Liu and Satou, 2019; Pasini et al., 2006; Roure and Darras, 2016; Shimeld et al., 2005; Wagner and Levine, 2012; Wagner et al., 2014), from the Aniseed database (Dardaillon et al., 2020) and from the present study, a list of 68 genes with expression in the palp lineage in *Ciona* and/or *Phallusia* (Table S3). We plotted the results of our *Phallusia* RNA-seq data, and found that 70% of the genes were regulated by BMP signaling. Most of them were repressed by BMP, but 20 genes were activated by BMP, and a smaller fraction was repressed or activated depending on the stage. Consequently, the precise function of BMP that is likely to be dynamic in the course of palp differentiation needs to be further investigated in details. Interestingly, Notch is likely to play a role in the specification of the different cell types that compose the palps. For instance, it has been shown that activating Notch represses palp neuronal markers in *H. roretzi* (Akanuma et al., 2002). We found 30 genes regulated by Notch in our dataset.

Discussion

We have shown that BMP signaling regulates two distinct steps of palp formation in *C. intestinalis*: ANB specification, and ventral papilla *vs* inter-papilla specification. Moreover, we have shown conservation of gene expression and regulation by BMP in *P. mammillata*.

Signaling pathway inhibition and ANB specification

ANB specification is regulated by inputs from several signaling pathways: FGF, Wnt and BMP. While FGF is positively required early on, at the time of neural induction (32-cell stage), all 3 pathways are inactive at the time of ANB fate acquisition as revealed by the expression of *Foxc* (mid-gastrula). This situation is reminiscent of data from vertebrates where anterior neural fate is determined by the triple inhibition of BMP, Nodal and Wnt pathways (Andoniadou and Martinez-Barbera, 2013; Niehrs et al., 2003; Wilson and Houart, 2004). It would thus be interesting to test the function of Nodal inhibition in ANB specification since we have already shown that it is involved in posterior neural fate determination in *Ciona* (Roure et al., 2014). While it appears that active FGF, Wnt or BMP signaling is incompatible with ANB determination, the specific function of each pathway seems different. FGF appears to regulate anterior CNS *vs* ANB fate decision along the antero-posterior axis (Wagner and Levine, 2012). Wnt seems to regulate *Foxc*+ ANB fate *vs Foxc*- ANB fate along the medio-lateral/dorso-ventral axis (Feinberg et al., 2019). Finally, BMP might participate in the segregation between ANB and immediately anterior/ventral epidermal fates. Finer details on the function of these pathways in ANB fate determination and on their likely cross-talk should be an exciting line of research in this simple and geometric model system.

From ANB to palp differentiation

Our results of late inhibition of BMP signaling (from gastrula stages) indicate that *Foxg*, expressed in a single row of cells with a U-shape, delineates cells competent to become papilla. A network of gene interactions has previously been identified that regulates the transition of *Foxg* from a U-shape to 3-spots eventually forming protruding papillae (Liu and Satou, 2019). BMP is an input to this network, presumably through the indirect regulation of ventral *Sp6/7/8/9* expression. We hypothesized the involvement of a signaling molecule that would be a direct target of BMP (Fig. 7). Interestingly, MAPK inhibition during neurulation results in a U-shaped expression of *Isl* (Wagner et al., 2014) similar to what we observed by

inhibiting BMP. It is tempting to propose an FGF ligand to be the factor downstream of BMP, however none has been described with a discrete pattern in the palps (Imai et al., 2004). Again, studying epistatic relationships and cross-talks between these signaling pathways is a future line of research.

Importantly, we have shown that BMP signaling is active and required in the median palp forming region, most likely corresponding to the future ventral palp, before the onset of *Foxg* and *Sp6/7/8/9* expression. However, activating BMP at this stage, does not result in ectopic palp formation but to an absence of the ventral palp. This discrepancy might be better understood by more finely controlling levels of BMP signaling but also its timing and cells that receive it, through optogenetics for example. Nevertheless, our observations point to differences between the two symmetrically bilateral dorsal palps and the single median ventral palp. While we are not aware of ventral palp-specific marker, we have shown that *Msx* is transiently expressed only in the ventral palp (Fig. 5); this may also be the case for *Hes.a* (Chowdhury et al., 2022). In addition, the *Pou4*+ sensory neurons are located dorsally in the ventral palp, while they are located around *Isl*+ cells in the dorsal palps. Specific dorsal and ventral genetic sub-network would thus be interesting to uncover.

Anterior adhesive organs formation in chordates.

The specification of the 3 cell types (ACCs, neurons and collocytes) that make the papillae and their relationships (lineage, alternative cell fate...) are still poorly understood, but will most likely be the subject of future research (Zeng et al., 2019). For example, we are not aware of collocytes specific gene marker, however these cells can be distinguished from other palp cells with the peanut agglutinin (Cao et al., 2019; Sato and Morisawa, 1999; Zeng et al., 2019). They are involved in the secretion of adhesive materials for the larva to attach to a substrate before metamorphosis. The palps thus constitute an adhesive organ whose homology with adhesive organs that exist in the larvae of some vertebrates (*e.g.* the cement gland of *Xenopus*) has been previously proposed (Yoshida et al., 2012). Our present work adds to the similarities observed between frog cement gland and ascidian palps: they are ectodermal derivatives specialized in adhesion, they are located at the anterior-most part of the larva, they share the expression of the transcription factors coding genes *Otx* and *Pitx*, and their formation is regulated by BMP signaling (Gammill and Sive, 2000; Jin and Weinstein, 2018; Yoshida et al., 2012). Further detailed comparison of the shared but also

426 divergent parts of the developmental networks regulating adhesive organ/sensory organ
427 formation in ascidians and vertebrates should be of great interest.
428
429 **Conservation of PNS formation in chordates?**
430 The ascidian larval PNS, palps included, originates from the neural plate border with the
431 exception of the ventral tail PNS that originates from a region at the opposite end of the
432 embryo, the ventral epidermis. Signaling pathways are pleiotropic and are consequently
433 poor indicators of possible evolutionary conservation. Nevertheless, it is striking that FGF,
434 Wnt and BMP are deployed in ascidians to regulate neural plate border specification and
435 differentiation of its derivatives, most likely with changing dynamic requirements at diverse
436 developmental stages. This is reminiscent of the mechanisms regulating neural plate border
437 and its derivatives, the cranial placodes and the neural crest (Martik and Bronner, 2021; Pla
438 and Monsoro-Burq, 2018; Stundl et al., 2021). The similarities extend beyond signaling
439 pathways since a suite of genes have conserved expression between ascidians and
440 vertebrates, and have led to several evolutionary scenarios (Cao et al., 2019; Horie et al.,
441 2018; Pasini et al., 2006; Poncelet and Shimeld, 2020). Our present study add material to
442 gene network level comparisons.
443 The ascidian PNS is made of epidermal sensory neurons that have different morphologies,
444 connectivity and sensory capacities depending on their location (Abitua et al., 2015; Imai and
445 Meinertzhagen, 2007; Ryan et al., 2018). However, they share a number of genes marking
446 the presumptive domains or differentiating neurons. Yet, what regulates their specific
447 identities is still incompletely understood (Chacha et al., 2022). For example, a number of
448 genes expressed in the tail PNS are also expressed in the palps, and these expression
449 domains are conserved in species that have diverged almost 400 My ago (Table S3)
450 (Akanuma et al., 2002; Coulcher et al., 2020; Joyce Tang et al., 2013; Pasini et al., 2006;
451 Roure and Darras, 2016). Comparative approaches of PNS formation between divergent
452 ascidian species and across chordates (vertebrates and cephalochordates) promise to yield
453 insights into PNS evolution and the flexibility of developmental mechanisms.
454
455

Materials and methods

Embryo obtention and manipulation

Adults from *Ciona intestinalis* (formerly referred to *Ciona intestinalis* type B (Brunetti et al., 2015)) were provided by the Centre de Ressources Biologiques Marines in Roscoff (EMBRC-France). Adults of *Phallusia mammillata* were provided by the Centre de Ressources Biologiques Marines in Banyuls-sur-mer (EMBRC-France) following diving or by professional fishermen following trawling in the Banyuls-sur-mer (France) area. Gametes collection, *in vitro* fertilization, dechorionation and electroporation were performed as previously described (Coulcher et al., 2020; Darras, 2021); and staging of embryos was performed according to the developmental table of *Ciona robusta* (Hotta et al., 2007).
Electroporation constructs used in this study have been previously described (Pasini et al., 2006). Embryos were treated with 150 ng/ml of recombinant mouse BMP2 protein (355-BEC, R&D Systems Inc, 100 µg/mL stock solution in HCl 4 mM + BSA 0.1 %), 100 ng/ml of recombinant human bFGF (F0291, Sigma-Aldrich, 50 µg/mL stock solution in 20 mM Tris pH=7.5 + BSA 0.1 %) complemented with 0.1% BSA, or 2.5 µM of the BMP receptor inhibitor DMH1 (S7146, Euromedex, 10 mM stock solution in DMSO) at the stages indicated in the text and figures. These concentrations were determined following pilot experiments. Control embryos were incubated with sea water containing 0.1 % BSA and/or 0.025% DMSO.

In situ hybridization and immunostaining

For all labeling experiments, embryos were fixed in 0.5 M NaCl, 100 mM MOPS pH=7.5 and 3.7% formaldehyde. Whole mount chromogenic *in situ* hybridization were performed using plasmid cDNA or synthetic DNA (eBlocks Gene Fragment, IDT) as templates for probe synthesis (Tables S2 and S4) as described previously (Chowdhury et al., 2022). Gene models and identifiers correspond to the following genome assemblies, KH2012 for *Ciona robusta* (Satou et al., 2008) and MTP2014 for *Phallusia mammillata*, that were retrieved from the Aniseed database (Dardaillon et al., 2020). Images were acquired using an AxioCam ERc5s digital camera mounted on a stereomicroscope (Discovery V20, Zeiss). The number of experiments and embryos for phenotypic effects by gene expression analysis are shown in the figures and their legends.

Fluorescent *in situ* hybridization were adapted from (Racioppi et al., 2014). Briefly, digoxigenin-labeled probes were recognized using an anti-DIG antibody coupled to peroxidase (11207733910, Roche), and fluorescein-labeled probes were recognized using an anti-FLUO antibody coupled to peroxidase (11426346910, Roche). Fluorescence signal was produced using the TSA plus kit (NEL753001KT, Perkin-Elmer) following manufacturer's recommendations with cyanin3 and fluorescein for DIG- and FLUO-probes respectively. Active BMP signaling was visualized by immunostaining using a rabbit monoclonal antibody against mammal Smad1, Smad5 and Smad8 phosphorylated at two serine residues at the C-terminal end (clone 41D10, #9516, Cell Signaling Technology) diluted at 1:200. The epitope is present in the single ortholog Smad1/5/8 of both *Ciona intestinalis* and *Phallusia mammillata*. Anti-rabbit coupled to Alexa Fluor 568 (A11011, Invitrogen) was used at 1:400 for visualization. Similar data were obtained using another antibody (clone D5B10, #13820, Cell Signaling Technology) (data not shown). Membranes were stained using Alexa Fluor 594 phalloidin (A12381, Invitrogen) used at 1:1000. Nuclei were stained using DAPI. Image acquisition was performed using confocal microscopy (Leica SP8-X, BioPiC platform, Banyuls-sur-mer). Confocal z-stacks were visualized and analyzed in 3D using the Imaris 8.3 software (Bitplane). In particular, this software was used to count the number of cells expressing a gene of interest. In brief, fluorescent signals were converted as 3D objects: *in situ* hybridization signals as surface objects, and DAPI-labeled nuclei as spots. The number of spots within a given surface was used as a proxy for the number of cells expressing a gene. Snapshots of such analyses and 3D renderings are shown in Figs 1,2,5,6,S1,S2. Maximum intensity projections of Fig. S4 were performed using ImageJ.

Image panels and figures were constructed with Affinity Photo and Affinity Designer.

Conflict of interest.

The authors declare that they have no conflict of interest.

Acknowledgements

We thank G. Diaz (Port-Vendres) and staff (M. Fuentes, divers and boat crew) at the marine stations of Banyuls-sur-mer and Roscoff (French node of the European research infrastructure EMBRC) for providing animals. We would like to acknowledge the BioPiC imaging facility (Sorbonne Université/CNRS, Banyuls-sur-mer), R. Dumollard and H. Yasuo for sharing plasmids, and V. Thomé for advices on fluorescent *in situ* hybridization and immunostaining.

Funding

AR and SD are CNRS staff. This work was supported by CNRS and Sorbonne Université, and by specific grants from the ANR (ANR-17-CE13-0027), the CNRS (DBM2020 from INSB) and the European project Assemble Plus (H2020-INFRAIA-1-2016–2017; Grant No. 730984).

Authors' contributions

AR and SD designed the project. AR performed most of the experiments and analyses with the help of RC and SD. SD supervised the project, wrote the manuscript and obtained funding. All authors edited the manuscript, read and approved the final version.

Data availability

RNA-seq data are available under the BioProject ID PRJNA779382. All other data generated or analyzed during this study are included in the manuscript and supporting files.

References

Abitua, P. B., Gainous, T. B., Kaczmarczyk, A. N., Winchell, C. J., Hudson, C., Kamata, K., Nakagawa, M., Tsuda, M., Kusakabe, T. G. and Levine, M. (2015). The pre-vertebrate origins of neurogenic placodes. *Nature* **524**, 462–465.

Akanuma, T., Hori, S., Darras, S. and Nishida, H. (2002). Notch signaling is involved in nervous system formation in ascidian embryos. *Dev Genes Evol* **212**, 459–72.

Andoniadou, C. L. and Martinez-Barbera, J. P. (2013). Developmental mechanisms directing early anterior forebrain specification in vertebrates. *Cell. Mol. Life Sci.* **70**, 3739–3752.

Brunetti, R., Gissi, C., Pennati, R., Caicci, F., Gasparini, F. and Manni, L. (2015). Morphological evidence that the molecularly determined *Ciona intestinalis* type A and type B are different species: *Ciona robusta* and *Ciona intestinalis*. *Journal of Zoological Systematics and Evolutionary Research* **53**, 186–193.

Cao, C., Lemaire, L. A., Wang, W., Yoon, P. H., Choi, Y. A., Parsons, L. R., Matese, J. C., Wang, W., Levine, M. and Chen, K. (2019). Comprehensive single-cell transcriptome lineages of a proto-vertebrate. *Nature* **571**, 349–354.

Chacha, P. P., Horie, R., Kusakabe, T. G., Sasakura, Y., Singh, M., Horie, T. and Levine, M. (2022). Neuronal identities derived by misexpression of the POU IV sensory determinant in a protovertebrate. *PNAS* **119**,.

Chen, J. S., Pedro, M. S. and Zeller, R. W. (2011). miR-124 function during Ciona intestinalis neuronal development includes extensive interaction with the Notch signaling pathway. *Development* **138**, 4943–4953.

Chowdhury, R., Roure, A., le Pétillon, Y., Mayeur, H., Daric, V. and Darras, S. (2022). Highly distinct genetic programs for peripheral nervous system formation in chordates. *BMC Biol* **20**, 1–25.

Cloney, R. A. (1977). Larval adhesive organs and metamorphosis in ascidians - I. Fine structure of the everting papillae of Distaplia occidentalis. *Cell and Tissue Research* **183**, 423–444.

Coulcher, J. F., Roure, A., Chowdhury, R., Robert, M., Lescat, L., Bouin, A., Carvajal Cadavid, J., Nishida, H. and Darras, S. (2020). Conservation of peripheral nervous system formation mechanisms in divergent ascidian embryos. *eLife* **9**, e59157.

Dardaillon, J., Dauga, D., Simion, P., Faure, E., Onuma, T. A., DeBiasse, M. B., Louis, A., Nitta, K. R., Naville, M., Besnardeau, L., et al. (2020). ANISEED 2019: 4D exploration of genetic data for an extended range of tunicates. *Nucleic Acids Res* **48**, D668–D675.

Darras, S. (2021). En masse DNA Electroporation for in vivo Transcriptional Assay in Ascidian Embryos. *Bio-protocol* **11**, e4160.

Darras, S. and Nishida, H. (2001). The BMP/CHORDIN antagonism controls sensory pigment cell specification and differentiation in the ascidian embryo. *Dev Biol* **236**, 271–88.

Delsuc, F., Brinkmann, H., Chourrout, D. and Philippe, H. (2006). Tunicates and not cephalochordates are the closest living relatives of vertebrates. *Nature* **439**, 965–8.

Delsuc, F., Philippe, H., Tsagkogeorga, G., Simion, P., Tilak, M.-K., Turon, X., López-Legentil, S., Piette, J., Lemaire, P. and Douzery, E. J. P. (2018). A phylogenomic framework and timescale for comparative studies of tunicates. *BMC Biology* **16**, 39.

Feinberg, S., Roure, A., Piron, J. and Darras, S. (2019). Antero-posterior ectoderm patterning by canonical Wnt signaling during ascidian development. *PLOS Genetics* **15**, e1008054.

Gammill, L. S. and Sive, H. (2000). Coincidence of otx2 and BMP4 signaling correlates with Xenopus cement gland formation. *Mechanisms of development* **92**, 217–226.

Guignard, L., Fiúza, U.-M., Leggio, B., Laussu, J., Faure, E., Michelin, G., Biasuz, K., Hufnagel, L., Malandain, G., Godin, C., et al. (2020). Contact area–dependent cell communication and the morphological invariance of ascidian embryogenesis. *Science* **369**,.
Horie, R., Hazbun, A., Chen, K., Cao, C., Levine, M. and Horie, T. (2018). Shared evolutionary origin of vertebrate neural crest and cranial placodes. *Nature* **560**, 228–232.
Hotta, K., Mitsuhara, K., Takahashi, H., Inaba, K., Oka, K., Gojobori, T. and Ikeo, K. (2007). A web-based interactive developmental table for the ascidian Ciona intestinalis, including 3D real-image embryo reconstructions: I. From fertilized egg to hatching larva. *Dev. Dyn.* **236**, 1790–1805.
Hudson, C. (2016). The central nervous system of ascidian larvae: Nervous system development in ascidians. *Wiley Interdisciplinary Reviews: Developmental Biology* **5**, 538–561.
Hudson, C., Darras, S., Caillol, D., Yasuo, H. and Lemaire, P. (2003). A conserved role for the MEK signalling pathway in neural tissue specification and posteriorisation in the invertebrate chordate, the ascidian Ciona intestinalis. *Development* **130**, 147–59.
Imai, J. H. and Meinertzhagen, I. A. (2007). Neurons of the ascidian larval nervous system in Ciona intestinalis: II. Peripheral nervous system. *The Journal of comparative neurology* **501**, 335–52.
Imai, K. S., Hino, K., Yagi, K., Satoh, N. and Satou, Y. (2004). Gene expression profiles of transcription factors and signaling molecules in the ascidian embryo: towards a comprehensive understanding of gene networks. *Development* **131**, 4047–58.
Imai, K. S., Levine, M., Satoh, N. and Satou, Y. (2006). Regulatory blueprint for a chordate embryo. *Science (New York, N.Y)* **312**, 1183–7.
Jin, Y. and Weinstein, D. C. (2018). Pitx1 regulates cement gland development in Xenopus laevis through activation of transcriptional targets and inhibition of BMP signaling. *Developmental Biology* **437**, 41–49.
Johnson, C. J., Razy-Krajka, F. and Stolfi, A. (2020). Expression of smooth muscle-like effectors and core cardiomyocyte regulators in the contractile papillae of Ciona. *EvoDevo* **11**, 15.
Joyce Tang, W., Chen, J. S. and Zeller, R. W. (2013). Transcriptional regulation of the peripheral nervous system in Ciona intestinalis. *Dev. Biol.* **378**, 183–193.
Kusakabe, T. G., Sakai, T., Aoyama, M., Kitajima, Y., Miyamoto, Y., Takigawa, T., Daido, Y., Fujiwara, K., Terashima, Y., Sugiuchi, Y., et al. (2012). A Conserved Non-Reproductive GnRH System in Chordates. *PLOS ONE* **7**, e41955.
Leggio, B., Laussu, J., Carlier, A., Godin, C., Lemaire, P. and Faure, E. (2019). MorphoNet: an interactive online morphological browser to explore complex multi-scale data. *Nat Commun* **10**, 2812.
Liu, B. and Satou, Y. (2019). Foxg specifies sensory neurons in the anterior neural plate border of the ascidian embryo. *Nat Commun* **10**, 4911.
Martik, M. L. and Bronner, M. E. (2021). Riding the crest to get a head: neural crest evolution in vertebrates. *Nat Rev Neurosci* 1–11.
Niehrs, C., Kazanskaya, O., Wu, W. and Glinka, A. (2003). Dickkopf1 and the Spemann-Mangold head organizer. *International Journal of Developmental Biology* **45**, 237–240.
Nishida, H. (1987). Cell lineage analysis in ascidian embryos by intracellular injection of a tracer enzyme. III. Up to the tissue restricted stage. *Dev Biol* **121**, 526–41.
Pasini, A., Amiel, A., Rothbacher, U., Roure, A., Lemaire, P. and Darras, S. (2006). Formation of the Ascidian Epidermal Sensory Neurons: Insights into the Origin of the Chordate Peripheral Nervous System. *PLoS Biol* **4**, e225.
Pennati, R. and Rothbächer, U. (2015). Bioadhesion in ascidians: a developmental and functional genomics perspective. *Interface Focus* **5**, 20140061.

Pla, P. and Monsoro-Burq, A. H. (2018). The neural border: Induction, specification and maturation of the territory that generates neural crest cells. *Developmental Biology* **444**, S36–S46.
Poncelet, G. and Shimeld, S. M. (2020). The evolutionary origins of the vertebrate olfactory system. *Open Biol.* **10**, 200330.
Racioppi, C., Kamal, A. K., Razy-Krajka, F., Gambardella, G., Zanetti, L., di Bernardo, D., Sanges, R., Christiaen, L. A. and Ristoratore, F. (2014). Fibroblast growth factor signalling controls nervous system patterning and pigment cell formation in Ciona intestinalis. *Nature Communications* **5**, 4830.
Rothbacher, U., Bertrand, V., Lamy, C. and Lemaire, P. (2007). A combinatorial code of maternal GATA, Ets and beta-catenin-TCF transcription factors specifies and patterns the early ascidian ectoderm. *Development (Cambridge, England)* **134**, 4023–32.
Roure, A. and Darras, S. (2016). Msxb is a core component of the genetic circuitry specifying the dorsal and ventral neurogenic midlines in the ascidian embryo. *Developmental Biology* **409**, 277–287.
Roure, A., Lemaire, P. and Darras, S. (2014). An Otx/Nodal Regulatory Signature for Posterior Neural Development in Ascidians. *PLoS Genetics* **10**, e1004548.
Ryan, K., Lu, Z. and Meinertzhagen, I. A. (2018). The peripheral nervous system of the ascidian tadpole larva: Types of neurons and their synaptic networks. *Journal of Comparative Neurology* **526**, 583–608.
Sato, Y. and Morisawa, M. (1999). Loss of test cells leads to the formation of new tunic surface cells and abnormal metamorphosis in larvae of Ciona intestinalis (Chordata, ascidiacea). *Development genes and evolution* **209**, 592–600.
Satoh, N. (1994). *Developmental biology of ascidians*. Cambridge University Press.
Satou, Y., Mineta, K., Ogasawara, M., Sasakura, Y., Shoguchi, E., Ueno, K., Yamada, L., Matsumoto, J., Wasserscheid, J., Dewar, K., et al. (2008). Improved genome assembly and evidence-based global gene model set for the chordate Ciona intestinalis: new insight into intron and operon populations. *Genome biology* **9**, R152.
Shimeld, S. M., Purkiss, A. G., Dirks, R. P. H., Bateman, O. A., Slingsby, C. and Lubsen, N. H. (2005). Urochordate βγ-Crystallin and the Evolutionary Origin of the Vertebrate Eye Lens. *Current Biology* **15**, 1684–1689.
Stundl, J., Bertucci, P. Y., Lauri, A., Arendt, D. and Bronner, M. E. (2021). Evolution of new cell types at the lateral neural border. In *Current Topics in Developmental Biology*, p. Academic Press.
Thawani, A. and Groves, A. K. (2020). Building the Border: Development of the Chordate Neural Plate Border Region and Its Derivatives. *Front. Physiol.* **11**,.
Wagner, E. and Levine, M. (2012). FGF signaling establishes the anterior border of the Ciona neural tube. *Development* **139**, 2351–2359.
Wagner, E., Stolfi, A., Gi Choi, Y. and Levine, M. (2014). Islet is a key determinant of ascidian palp morphogenesis. *Development* **141**, 3084–3092.
Waki, K., Imai, K. S. and Satou, Y. (2015). Genetic pathways for differentiation of the peripheral nervous system in ascidians. *Nature Communications* **6**, 8719.
Wilson, S. W. and Houart, C. (2004). Early Steps in the Development of the Forebrain. *Developmental Cell* **6**, 167–181.
Yoshida, K., Ueno, M., Niwano, T. and Saiga, H. (2012). Transcription regulatory mechanism of Pitx in the papilla-forming region in the ascidian, Halocynthia roretzi, implies conserved involvement of Otx as the upstream gene in the adhesive organ development of chordates. *Development, Growth & Differentiation* **54**, 649–659.
Zeng, F., Wunderer, J., Salvenmoser, W., Hess, M. W., Ladurner, P. and Rothbächer, U. (2019). Papillae revisited and the nature of the adhesive secreting collocytes. *Developmental*

687 *Biology* **448**, 183–198.
688
689

690 **Figure legends**

691

692 **Figure 1. Early BMP activation prevents palp formation.** BMP pathway was activated by
693 overexpressing the BMP ligand Admp using the *Fog* ectodermal promoter. Experimental
694 embryos were compared to control (overexpressing the fluorescent protein Venus). **(A-D)**
695 Papilla protrusions and elongated cells were absent following BMP activation as revealed by
696 confocal stacks for phalloidin (white) and DAPI (cyan) staining at larval stages (A,B: confocal
697 sections; C,D: surface rendering). Scale bar: 20 µm. **(E-V)** BMP activation repressed genes
698 expressed in the palps as determined by *in situ* hybridization for *Sp6/7/8/9* (E,F), *Isl* (G,H),
699 *Foxg* (I,J), *Celf3/4/5/6* (K,L), *Pou4* (M,N) and *Emx* (O,P) at mid-tailbud stages (St. 23); and
700 *Foxg* (Q,R) and *Foxc* (U,V) at neurula stages. The expression of the epidermis marker
701 *Sox14/15/21* which is excluded from the palps at neurula stages was unchanged (S,T). For
702 each panel, n indicates the number of embryos examined. The percentages correspond to
703 normal expression for pFog>Venus, and to gene repression (except for *Sox14/15/21*) in the
704 palp territory for pFog>Admp. Experiments have been performed at least twice, except for
705 *Celf3/4/5/6*, *Pou4*, *Emx* and *Sox14/15/21* where results come from a single experiment. In
706 tailbud embryos, a bulging mass of cells was often visible in the dorsal posterior trunk. It
707 most likely corresponds to the CNS as revealed by *Celf3/4/5/6* expression that was outside
708 of the embryo due to abnormal neural tube closure. Anterior to the left in lateral views
709 except Q-T (frontal views) and U-V (neural plate views). Scale bar: 50 µm. **(W-X)** Schematic
710 representation of the progeny of the neural plate: CNS in orange, palp region in light purple
711 and aATENS (sensory neurons of the trunk PNS) precursors in gray (adapted from (Horie et
712 al., 2018; Liu and Satou, 2019)).

713

714 **Figure 2. Dynamic BMP activity in the palp forming region. (A-E)** P-Smad1/5/8
715 immunostaining (magenta) at various developmental stages in control embryos: (A) early
716 gastrula (St. 11, vegetal view), (B) late gastrula (St. 13, ventral view), (C) neurula (St. 14/15,
717 ventral view), (D) initial tailbud (St. 18, lateral view), and (E) late tailbud (St. 23, lateral view)
718 stages. **(F-J)** P-Smad1/5/8 immunostaining (magenta) and *in situ* hybridization (green) for
719 *Foxc* at early neurula stages (St. 14) (F,G), and *Foxg* at late neurula (St. 16) (H,I) and mid
720 tailbud (St. 21) (J) stages of control embryos. Dorsal is to the top with lateral views and
721 anterior to the left (F,H,J), or frontal views (G,I). F and G are different views of the same

embryo. H and I are different views of another embryo. All data have been obtained from at least two independent experiments. Scale bar: 20 µm. The embryos have been outlined with white dotted lines. **(K)** Schematic representation of the dynamics of P-Smad1/5/8 (magenta circles) with respect to the palp forming region (light purple). The schemes depict sagittal sections with anterior to the left and dorsal to the top at early gastrula (St. 10/11), late gastrula (St.13), early neurula (St. 14), late neurula (St. 16) and mid tailbud (St. 21) stages. Main sites of expression are depicted: a few endomesodermal cells (St. 10/11), posterior ventral epidermis and endoderm (St. 13), ventral epidermis and endoderm throughout the antero-posterior axis (St. 14 and 16), ventral part of the palp forming region (St 16 and 21), trunk ventral epidermis, endoderm and sensory vesicle (St 21). **(L)** Active BMP signaling (P-Smad1/5/8 in magenta) and palp gene expression (green) for *Foxc*, *Foxg* and *Sp6/7/8/9* were mapped to schematic embryos according to the above data and previous reports (Horie et al., 2018; Liu and Satou, 2019). Schemes and lineages representing the frontal view of embryos during gastrulation and neurulation were drawn following *Phallusia mammillata* 4D reconstructions available at https://morphonet.org/ (Guignard et al., 2020; Leggio et al., 2019).

Figure 3. Inactive BMP signaling is required for ANB specification. (A-C) *Foxc* expression by *in situ* hybridization at early neurula stages (St. 14) was unchanged following BMP pathway inhibition by Noggin overexpression (B) or DMH1 treatment from the 8-cell stage (C). **(D-G)** Embryos were treated from the 8-cell stage to the fixation at early neurula stages (St. 14) with BMP2 protein or DMH1 alone, or in combination with bFGF protein. Gene expression was assessed by *in situ* hybridization for *Celf3/4/5/6* (D), *Otx* (E), *Tfap2-r.b* (F) and *Foxc* (G). For each panel, n indicates the number of embryos examined. The percentages indicate the frequency of the phenotype depicted in the picture. The results come from two independent experiments. Embryos are shown with anterior to the left in neural plate views except insets that are lateral views with dorsal to the top. The arrows in Dii and Eii mark the downregulation of *Celf3/4/5/6* and *Otx* in the palp precursors. Scale bar: 50 µm. **(H)** Schematic interpretations of the consequences of the various treatments (i: control, ii: BMP2, iii: DMH1, iv: bFGF, v: BMP2+bFGF and vi: DMH1+bFGF) on some ectodermal derivatives: palp precursors (light purple), a-line neural tissue (orange), a-line epidermis (light gray) and b-line epidermis (dark grey). The embryo schemes show a neural plate view (top) and a

lateral view (bottom) with anterior to the left. The schemes were drawn using *Phallusia mammillata* 4D reconstructions available at https://morphonet.org/ (Guignard et al., 2020; Leggio et al., 2019).

Figure 4. Late effects of BMP pathway modulations on palp formation. Embryos were treated with BMP2 protein (left panels) or DMH1 (right panels) from the stage indicated on the figure up to fixation and *in situ* hybridization for *Foxc* at early neurula stages (St. 14) and *Isl* at late tailbud stages (St. 23). For each panel, n indicates the number of embryos examined. The percentages indicate the frequency of the phenotype depicted in the picture. The results come from two or more independent experiments. Embryos are shown in neural plate views with anterior to the left for *Foxc* and frontal view with dorsal to the top for *Isl*. White arrowheads highlight the absence of the ventral spot of *Isl*. Scale bar: 50 µm.

Figure 5. BMP inhibition leads to the formation of a single large palp of dorsal character. **(A-P)** Embryos where BMP signaling was inhibited using treatment with DMH1 from St. 10 (E,G,H,M-P)) or Noggin overexpression (F) were compared to control embryos (A-D,I-L) for morphology and gene expression by *in situ* hybridization. *Isl*, normally expressed in each of the 3 protruding palps (A; 86%, n=7), was expressed as a large spot in a single protrusion at late tailbud stages (St. 25) in treated embryos (E; 100%, n=21). The single large protrusion is made of elongated cells (F-H; DAPI in cyan and phalloidin in white). Double fluorescent *in situ* hybridization for *Pou4* (magenta) and *Isl* (green) in control (I) and treated embryo (M) at late tailbud stages (St. 23). 3D representation of nuclei for cells expressing each gene (J,N). Double fluorescent *in situ* hybridization for *Msx* (magenta) and *Isl* (green) in control (K) and treated embryo (O) at early tailbud stages (St. 19). 3D representation of nuclei for cells expressing each gene (L,P). Co-expression of *Isl* and *Msx* appears white. Embryos are shown with dorsal to the top in lateral views (A-H) or frontal views (I-P). Scale bars: 50 µm, except for D and H: 20 µm. **(Q)** Count of the number of cells expressing each gene at late tailbud stages (St. 23) using 3D reconstructions as in J and N. The graph represents the average values from two or more independent experiments, with error bars denoting the standard deviation. Differences in cell number were evaluated using the Mann-Whitney U test, and p-values are indicated (n.s.: non statistically significant). The numbers of embryos examined

785 are as follows: control embryos (*Isl*: 14, *Pou4*: 5, *Celf3/4/5/6*: 5, and *Sp6/7/8/9*: 6) and
786 DMH1-treated embryos (*Isl*: 9, *Pou4*: 6, *Celf3/4/5/6*: 5, and *Sp6/7/8/9*: 5).
787
788 **Figure 6. Late BMP activation prevents ventral palp formation.** Embryos for which BMP
789 signaling was activated using BMP2 treatment from St. 10 (G-L) were compared to control
790 embryos (A-F) for morphology and gene expression by *in situ* hybridization. While 3
791 protruding papillae made of elongated cells were clearly seen in control embryos (A-B), only
792 2 dorsal protruding papillae were present in treated larvae (G-H) (B,H: phalloidin (white) and
793 DAPI (cyan) in confocal sections; A,G: resulting surface rendering). **(C,I)** Double fluorescent *in*
794 *situ* hybridization for *Pou4* (magenta) and *Isl* (green) in control (C) and treated embryo (I) at
795 late tailbud stages (St. 23). While 3 spots of *Isl* expression were seen in control embryos
796 (n=3), 2 dorsal spots were detected in all treated embryos (n=4). In the ventral region, *Pou4*
797 was expressed in 2 cells in controls (as described in Fig. 5). In treated embryos, we found 2
798 embryos with 2 $Pou4^{+}$ cells and 2 embryos with 1 $Pou4^{+}$ cell. White arrows in I point to two
799 $Pou4^{+}$ cells in the ventral area of a treated embryo. **(D,J)** Fluorescent *in situ* hybridization for
800 *Msx* (magenta) in control (D) and treated embryo (J) at early tailbud stages (St. 19). Control
801 embryos: 100% with *Msx* expression in the ventral palp region (n=4). BMP2-treated
802 embryos: 100% without *Msx* expression (n=12). **(E,F,K,L)** Colorimetric *in situ* hybridization for
803 *Sp6/7/8/9* (E,K) and *Sox14/15/21* (F,L). In these panels, n indicates the number of embryos
804 examined. The percentages indicate the frequency of the phenotype depicted in the picture
805 (the results come from two independent experiments). White stars in I-K highlight the
806 absence of staining in the ventral region. Embryos are shown with dorsal to the top in frontal
807 views except lateral views in B and H. Scale bars: 25 µm (displayed for each type of imaging
808 data).
809
810 **Figure 7. Regulation of *Foxg* and *Sp6/7/8/9* by BMP signaling. (A-D)** Expression of *Foxg* at
811 different developmental stages in the palp forming area (the specific stage is indicated at the
812 top of each picture). Note that, at early stages (A), *Foxg* was expressed in two anterior
813 ectodermal territories, the U-shaped palp forming region and a more dorsal row of cells
814 likely contributing to the oral siphon primordium (Liu and Satou, 2019). At initial tailbud
815 stages (B) *Foxg* expression was dramatically downregulated in the U-shaped region.
816 Concomitantly, a transient strong expression in the ventral trunk epidermis was detected.

817 **(E)** At mid tailbud stages, *Foxg* was expressed following a U-shape when BMP pathway was
818 inhibited from early gastrula (St. 10) with DMH1. **(F-H)** *Sp6/7/8/9* expression at different
819 developmental stages in the palp forming area. **(I-T)** Expression of *Foxg* (I-K) at late neurula
820 stages (St. 16) and *Sp6/7/8/9* (L-N) at initial tailbud stages (St. 18) in control embryos (I,L),
821 BMP2-treated embryos (J,M), and DMH1-treated embryos (K,N). n indicates the number of
822 embryos examined. The percentages indicate the frequency of the phenotype depicted in
823 the picture. The results come from two independent experiments. Embryos are shown in
824 frontal view with dorsal to the top. Scale bar: 50 µm. A schematic representation of our
825 interpretation of the expression patterns is shown for *Foxg* (O-Q) and *Sp6/7/8/9* (R-T) with
826 the same color code as in Fig. 2 (light purple: palp precursors; orange: a-line CNS; gray:
827 aATEN precursors; and green: gene expression). **(U-X)** Model for the action of BMP signaling
828 on protruding papilla *vs* inter-palp fate specification. The model focuses on the 8 *Foxg*$^{+}$ cells
829 making a U-shape at neurula stages that have the potential to become protruding papillae.
830 Importantly, dorsal palp formation is independent of BMP signaling, and expression data (I-
831 N) show that only the 4 median cells are affected by BMP signaling. Hence, the model
832 focuses only on these 4 cells where we postulate some genetic interactions (U). During
833 normal development (V), active BMP signaling (magenta) in the two median cells induces
834 ventral fate and the expression of an unidentified factor (green) that activates the
835 expression of *Sp6/7/8/9* (yellow) in the neighboring cells (*Sp6/7/8/9* is also activated
836 independently of BMP in the most dorsal cells). Next, Sp6/7/8/9 represses the expression of
837 *Foxg* (light purple) leading to alternate and excluded patterns of expression of these two
838 genes and subsequent specification of protruding and non-protruding cells. Following BMP
839 activation (W), the unidentified factor activates *Sp6/7/8/9* in the 4 median cells, abolishing
840 *Foxg* expression and the formation of the ventral protrusion. In absence of BMP signaling (X),
841 median cells do not acquire a ventral identity and do not express the unidentified factor.
842 Hence *Sp6/7/8/9* expression is not activated and *Foxg* not repressed.
843
844 **Figure 8. The BMP signaling pathway regulates palp formation in *Phallusia mammillata*.**
845 **(A)** Schematic representation of the appearance of adults *C. intestinalis* and *P. mammillata*,
846 and their phylogenetic distance. **(B-N)** *P. mammillata* embryos were treated from the 8-cell
847 stage with 150 ng/ml recombinant BMP2 protein (C,F,J,N) or 2.5 µM DMH1 (D,G,H,K,L). They
848 were fixed at neurula stages (B-D) and mid/late tailbud stages (E-N). Expression patterns for

CeIf3/4/5/6 (B-H), *Isl* (I-L) and *Pou4* (M,N) was determined by *in situ* hybridization. The arrow in C marks the repression of *CeIf3/4/5/6* in the ANB. For each panel, n indicates the number of embryos examined. The percentages indicate the frequency of the phenotype depicted in the picture. The results come from two or more independent experiments. Embryos are shown with anterior to the left in neural plate view (B-D), and in frontal view with dorsal to the top (E-N). Scale bar: 50 µm.

Figure 9. Identification of genes expressed in the palps in *Phallusia mammillata*. *In situ* hybridization at selected stages for *Chrdl* (A), *Tp53inp* (B,C), *Fzd9/10* (D,E), *Plg* (F,G), *Mucin* (H), *Hes.b* (I), *Barhl* (J), *Nos* (K), *Fbn* (L) and *Wscd* (M). Embryos are shown with anterior to the left in neural plate view (A,B,D), in lateral view with dorsal to the top (B inset,C,D inset, E-M), and in frontal view with dorsal to the top (insets in C,E,F,H,L,M). Scale bar: 50 µm.

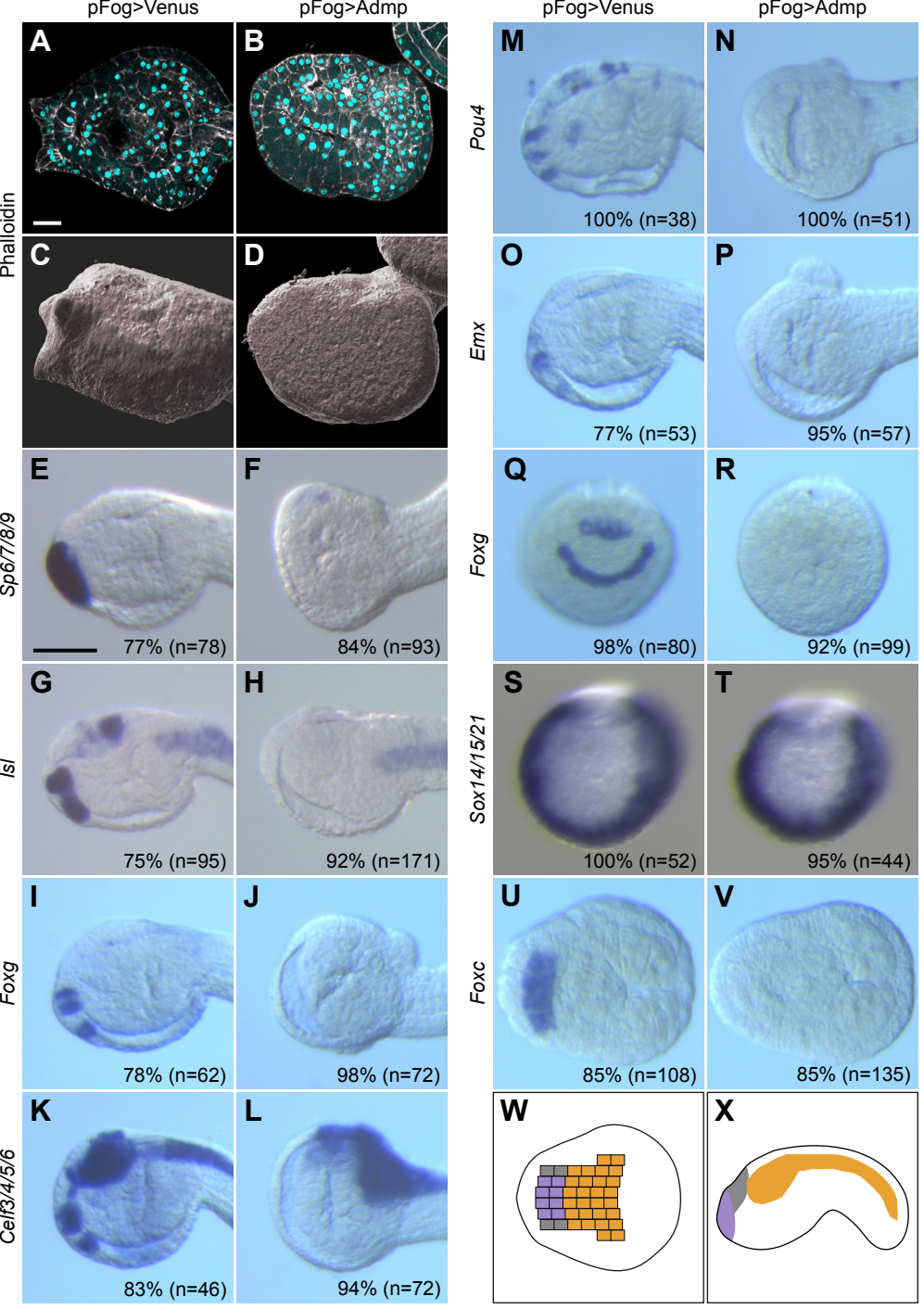
pFog>Venus
pFog>Admp
pFog>Venus
pFog>Admp
Phalloidin
A
B
C
D
M
N
Pou4
100% (n=38)
100% (n=51)
O
P
Emx
77% (n=53)
95% (n=57)
Sp6/7/8/9
E
F
77% (n=78)
84% (n=93)
Q
R
Foxg
98% (n=80)
92% (n=99)
Isl
G
H
75% (n=95)
92% (n=171)
S
T
Sox14/15/21
100% (n=52)
95% (n=44)
Foxg
I
J
78% (n=62)
98% (n=72)
U
V
Foxc
85% (n=108)
85% (n=135)
Celf3/4/5/6
K
L
83% (n=46)
94% (n=72)
W
X

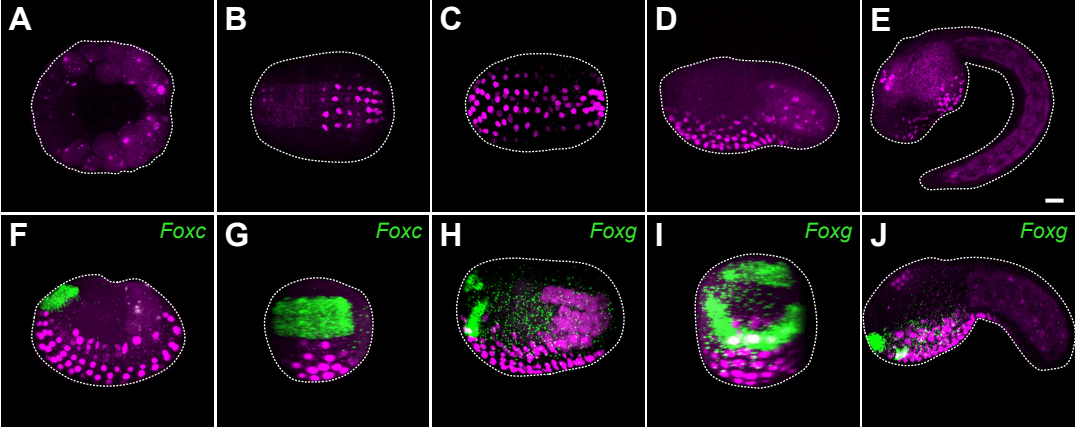
A
B
C
D
E
F
Foxc
G
Foxc
H
Foxg
I
Foxg
J
Foxg

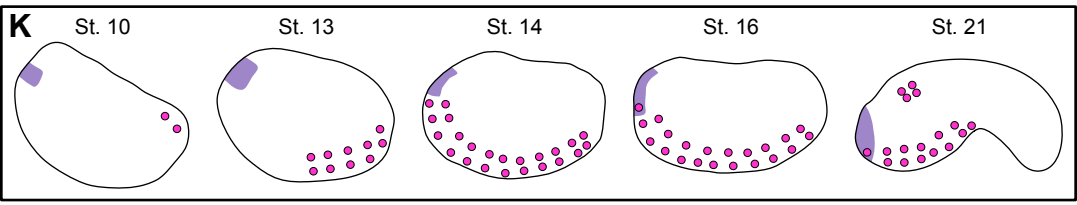
K
St. 10
St. 13
St. 14
St. 16
St. 21

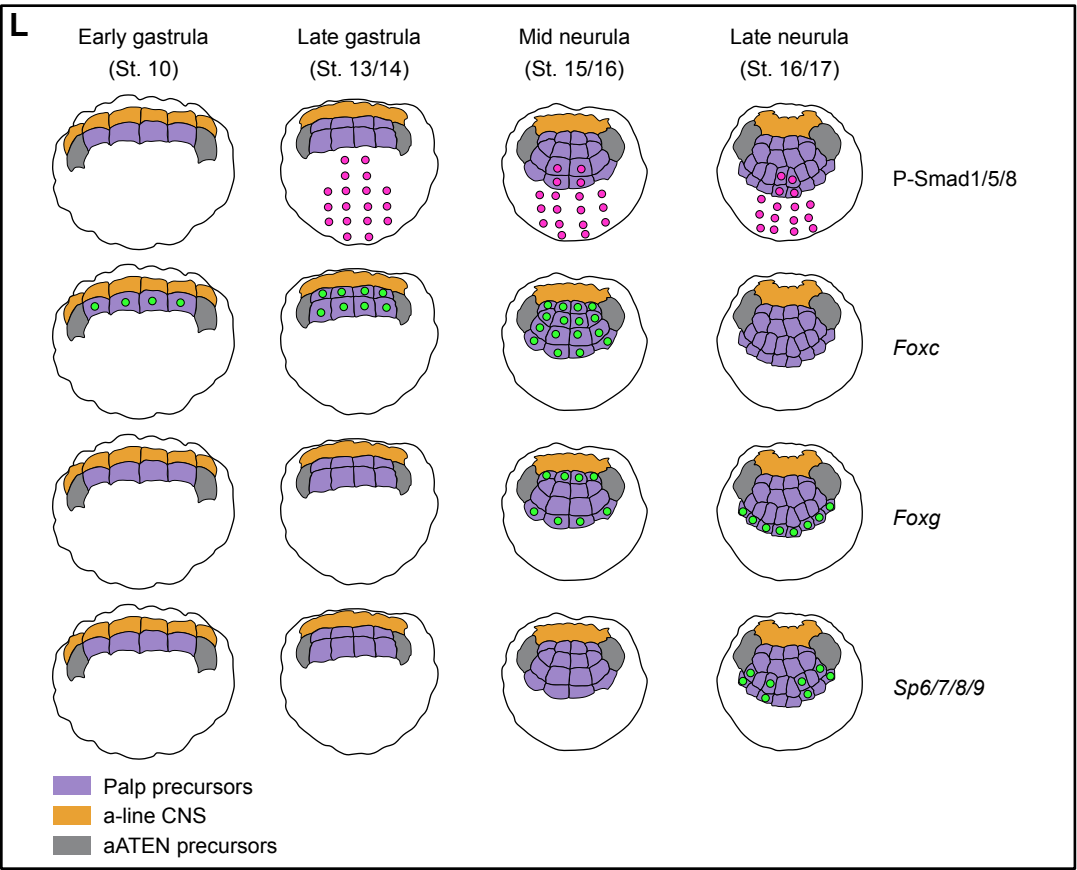
L
Early gastrula
(St. 10)
Late gastrula
(St. 13/14)
Mid neurula
(St. 15/16)
Late neurula
(St. 16/17)
P-Smad1/5/8
Foxc
Foxg
Sp6/7/8/9
Palp precursors
a-line CNS
aATEN precursors

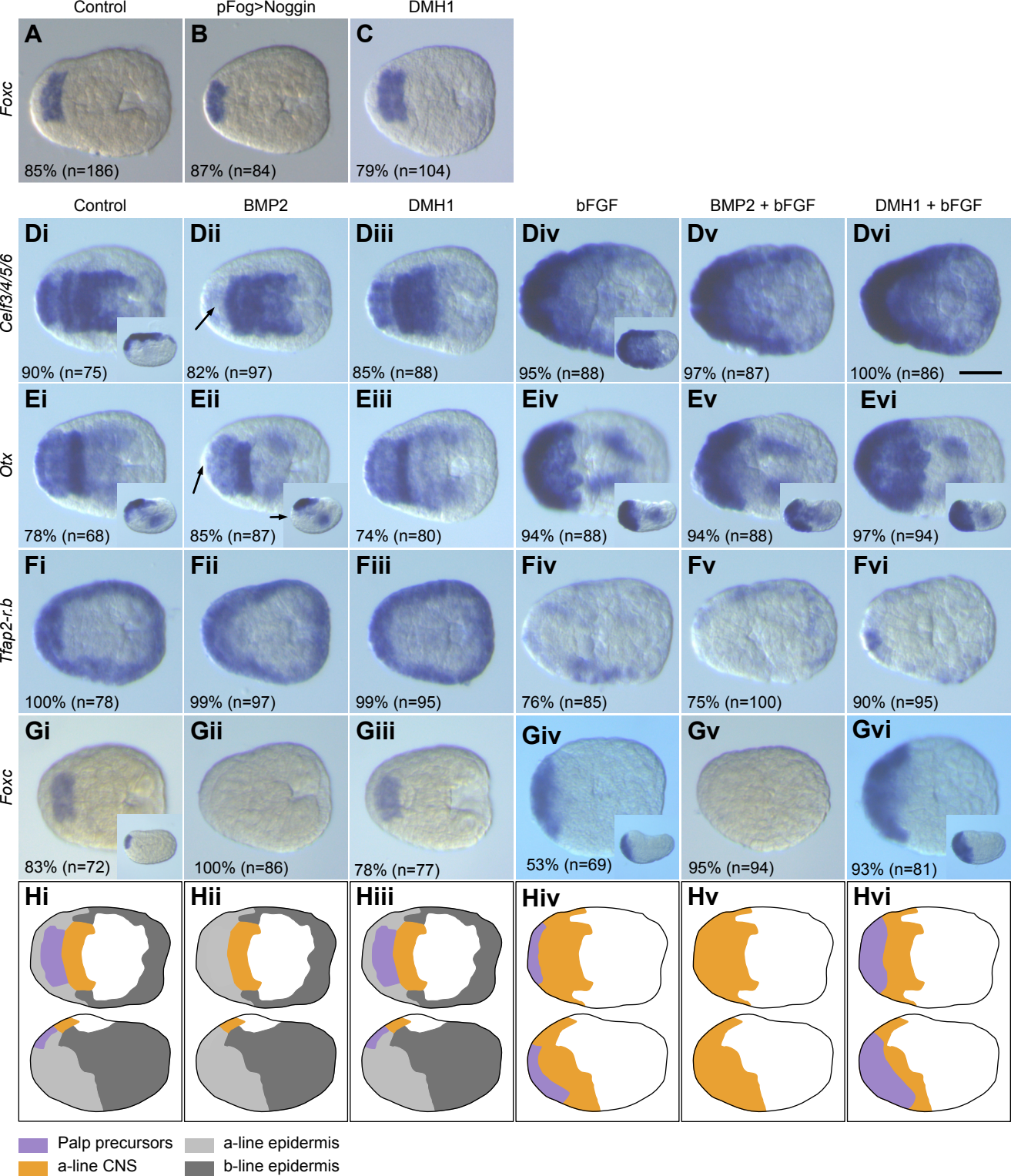
Control
pFog>Noggin
DMH1
Foxc
A
85% (n=186)
B
87% (n=84)
C
79% (n=104)
Control
BMP2
DMH1
bFGF
BMP2 + bFGF
DMH1 + bFGF
Celf3/4/5/6
Di
90% (n=75)
Dii
82% (n=97)
Diii
85% (n=88)
Div
95% (n=88)
Dv
97% (n=87)
Dvi
100% (n=86)
Otx
Ei
78% (n=68)
Eii
85% (n=87)
Eiii
74% (n=80)
Eiv
94% (n=88)
Ev
94% (n=88)
Evi
97% (n=94)
Tfap2-r.b
Fi
100% (n=78)
Fii
99% (n=97)
Fiii
99% (n=95)
Fiv
76% (n=85)
Fv
75% (n=100)
Fvi
90% (n=95)
Foxc
Gi
83% (n=72)
Gii
100% (n=86)
Giii
78% (n=77)
Giv
53% (n=69)
Gv
95% (n=94)
Gvi
93% (n=81)
Hi
Hii
Hiii
Hiv
Hv
Hvi
Palp precursors
a-line CNS
a-line epidermis
b-line epidermis

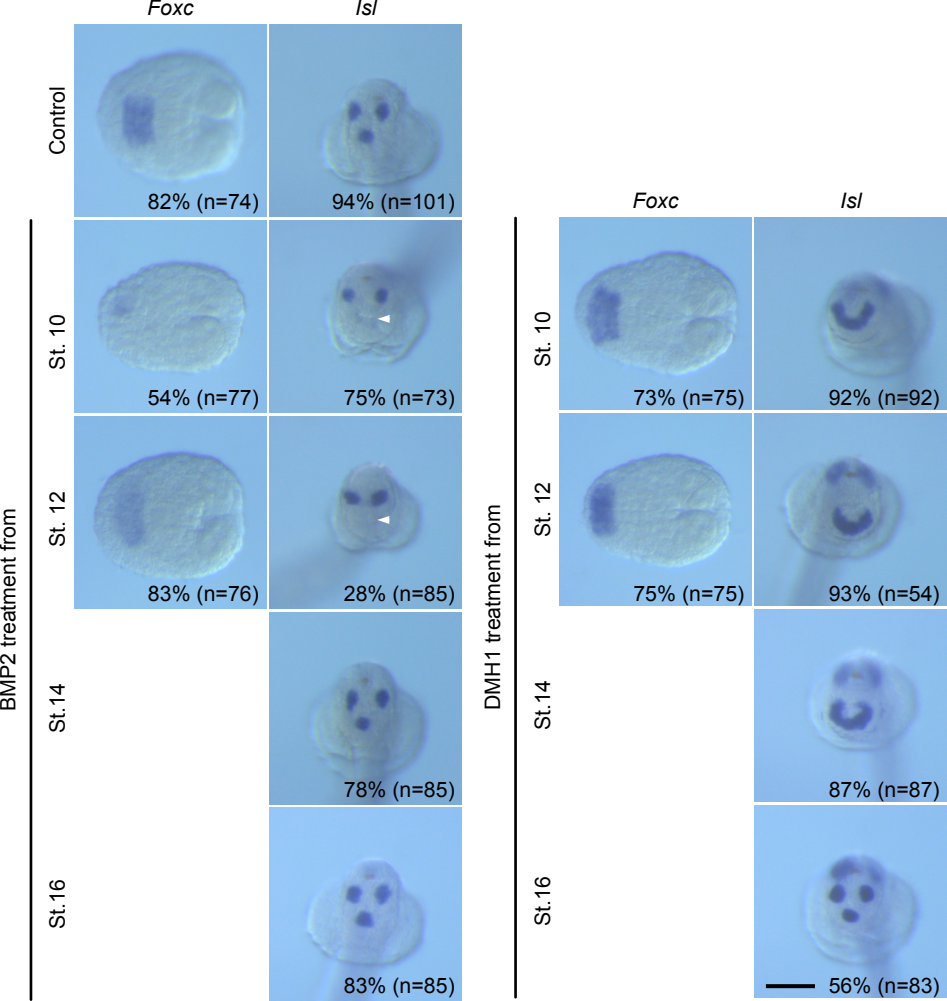
Foxc
Isl
Control
82% (n=74)
94% (n=101)
BMP2 treatment from
St. 10
54% (n=77)
75% (n=73)
St. 12
83% (n=76)
28% (n=85)
St.14
78% (n=85)
St.16
83% (n=85)
DMH1 treatment from
Foxc
Isl
St. 10
73% (n=75)
92% (n=92)
St. 12
75% (n=75)
93% (n=54)
St.14
87% (n=87)
St.16
56% (n=83)

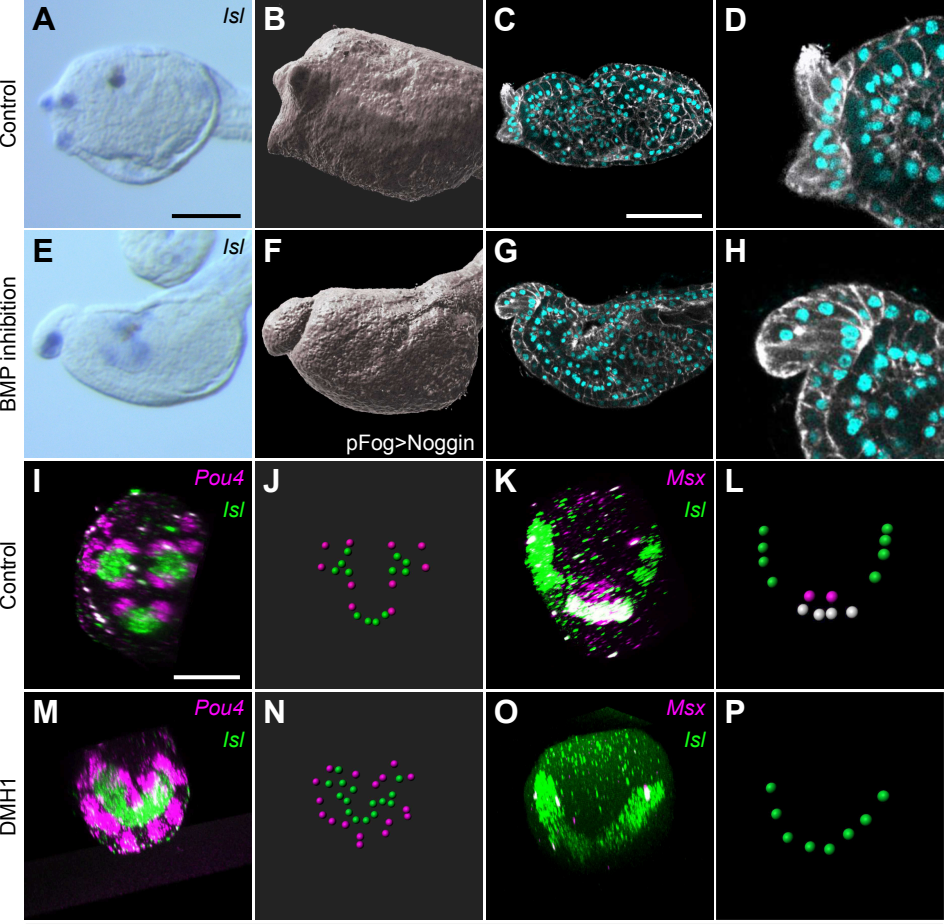
A
Isl
B
C
D
Control
E
Isl
F
pFog>Noggin
G
H
BMP inhibition
I
Pou4
Isl
J
K
Msx
Isl
L
Control
M
Pou4
Isl
N
O
Msx
Isl
P
DMH1

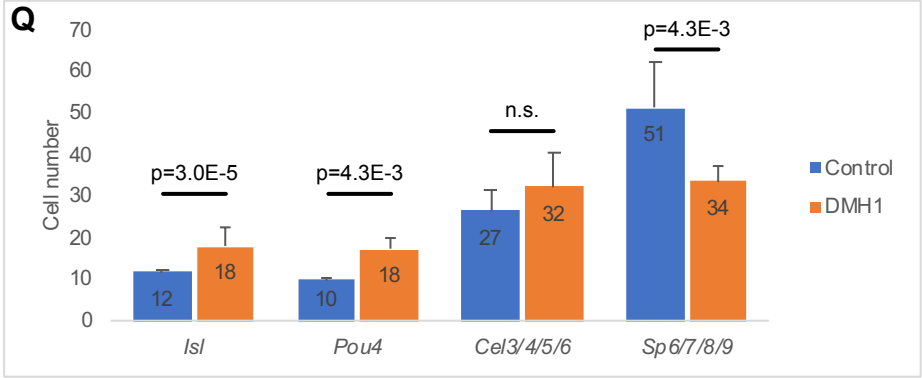
Q
Cell number
70
60
50
40
30
20
10
0
p=3.0E-5
p=4.3E-3
n.s.
p=4.3E-3
12
18
10
18
27
32
51
34
Isl
Pou4
Cel3/4/5/6
Sp6/7/8/9
Control
DMH1

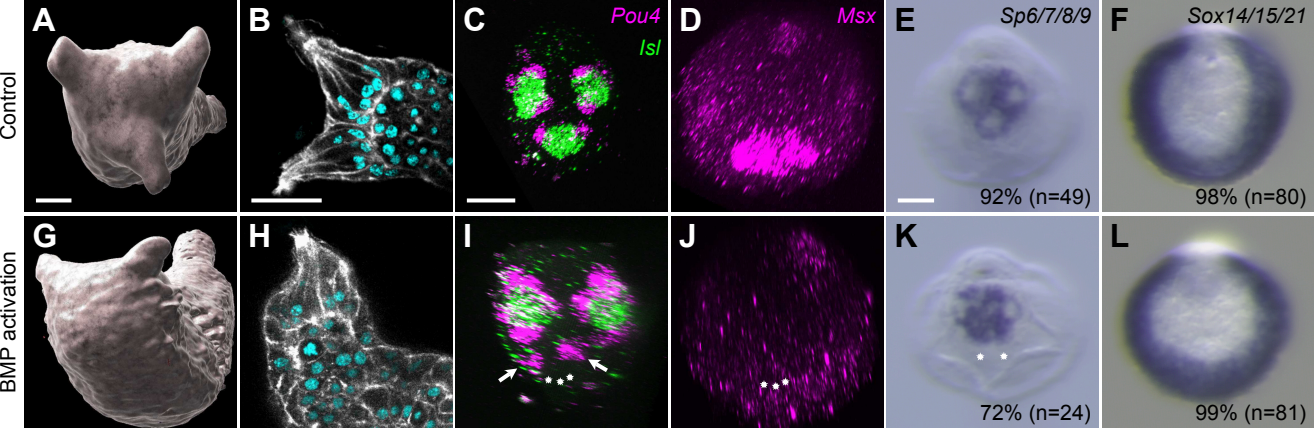
Control
BMP activation
A
B
C
Pou4
Isl
D
Msx
E
Sp6/7/8/9
92% (n=49)
F
Sox14/15/21
98% (n=80)
G
H
I
J
K
72% (n=24)
L
99% (n=81)

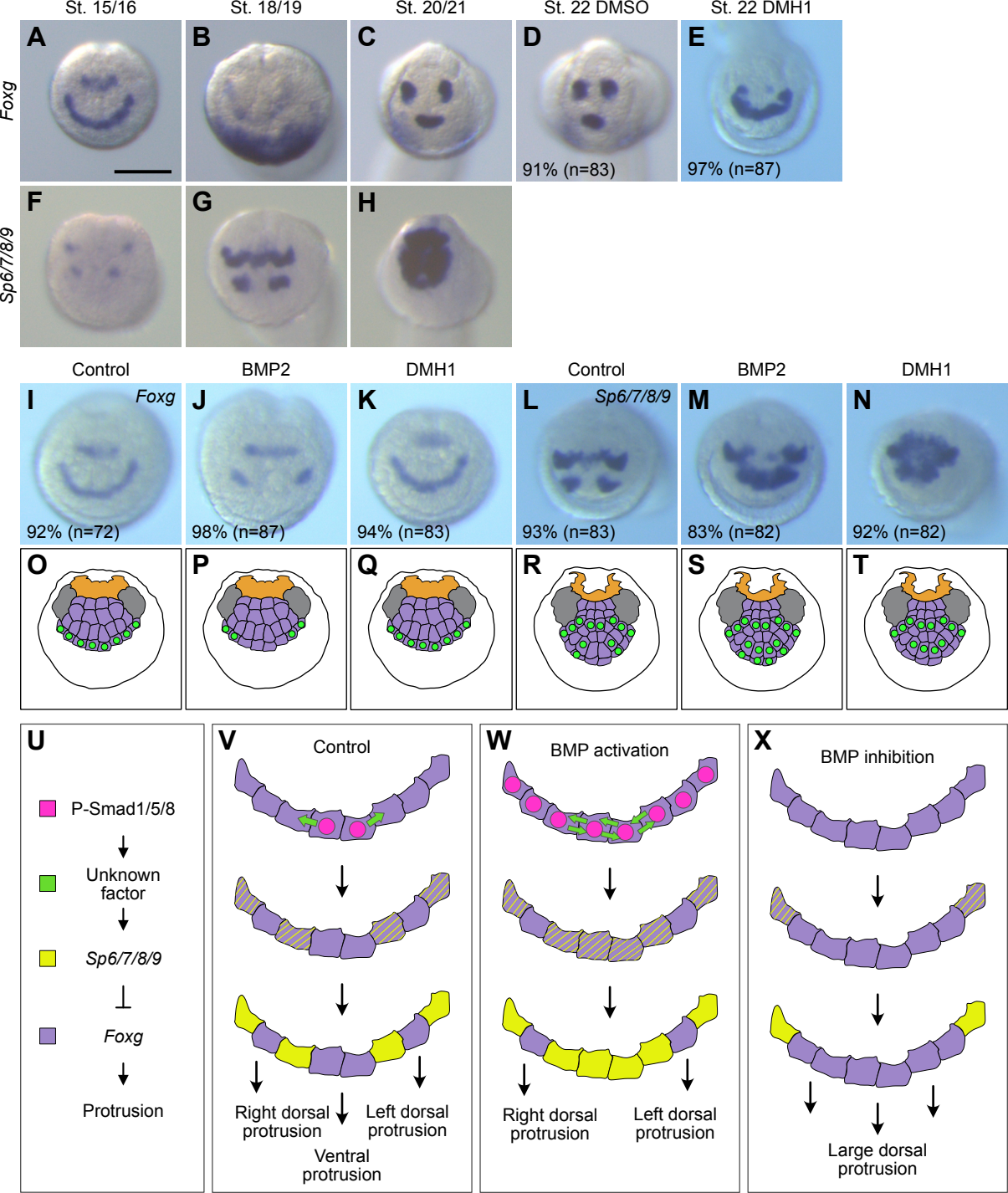
St. 15/16
St. 18/19
St. 20/21
St. 22 DMSO
St. 22 DMH1
Foxg
Sp6/7/8/9
A
B
C
D
E
F
G
H
91% (n=83)
97% (n=87)
Control
BMP2
DMH1
Control
BMP2
DMH1
I
J
K
L
M
N
Foxg
Sp6/7/8/9
92% (n=72)
98% (n=87)
94% (n=83)
93% (n=83)
83% (n=82)
92% (n=82)
O
P
Q
R
S
T
U
P-Smad1/5/8
Unknown factor
Sp6/7/8/9
Foxg
Protrusion
V
Control
Right dorsal protrusion
Left dorsal protrusion
Ventral protrusion
W
BMP activation
Right dorsal protrusion
Left dorsal protrusion
X
BMP inhibition
Large dorsal protrusion

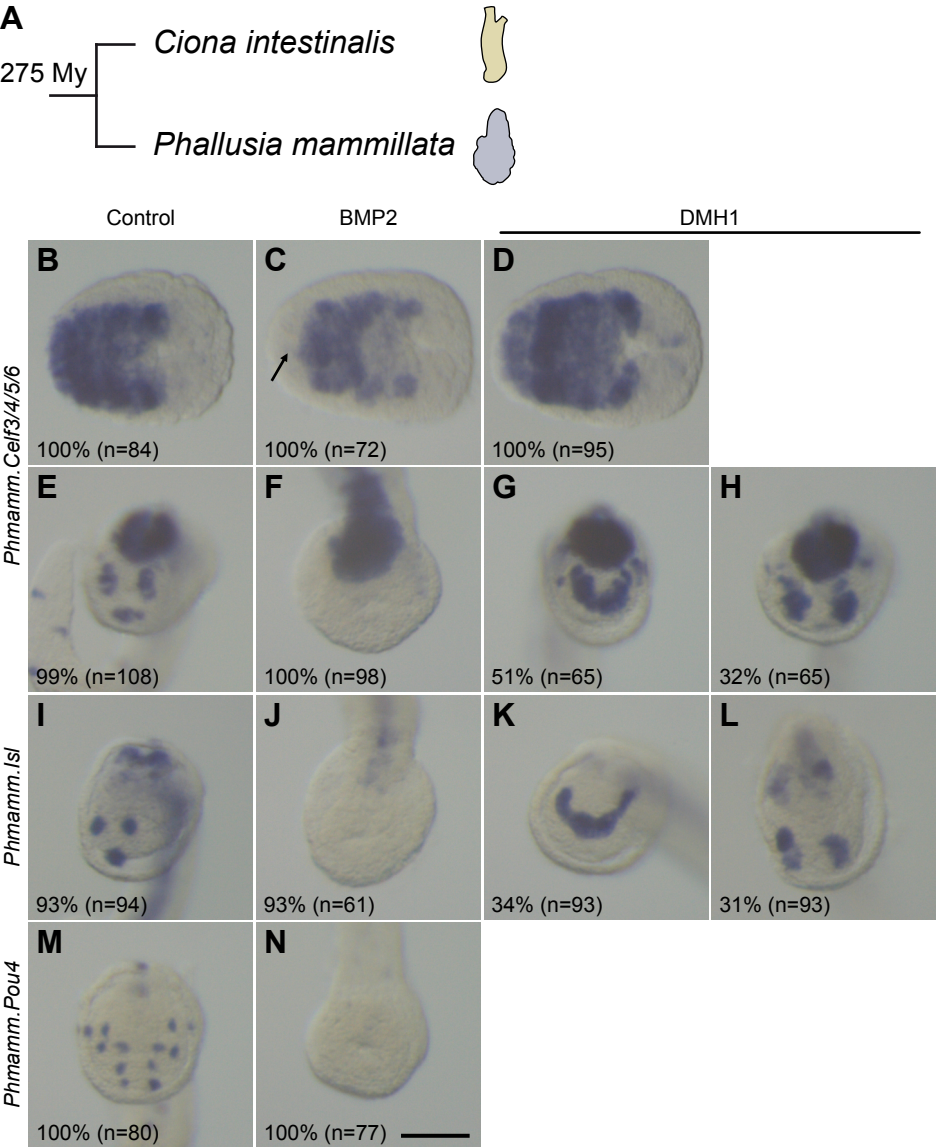
A
Ciona intestinalis
275 My
Phallusia mammillata
Control
BMP2
DMH1
B
C
D
100% (n=84)
100% (n=72)
100% (n=95)
Phmamm.Celf3/4/5/6
E
F
G
H
99% (n=108)
100% (n=98)
51% (n=65)
32% (n=65)
I
J
K
L
93% (n=94)
93% (n=61)
34% (n=93)
31% (n=93)
Phmamm.Isl
M
N
100% (n=80)
100% (n=77)
Phmamm.Pou4

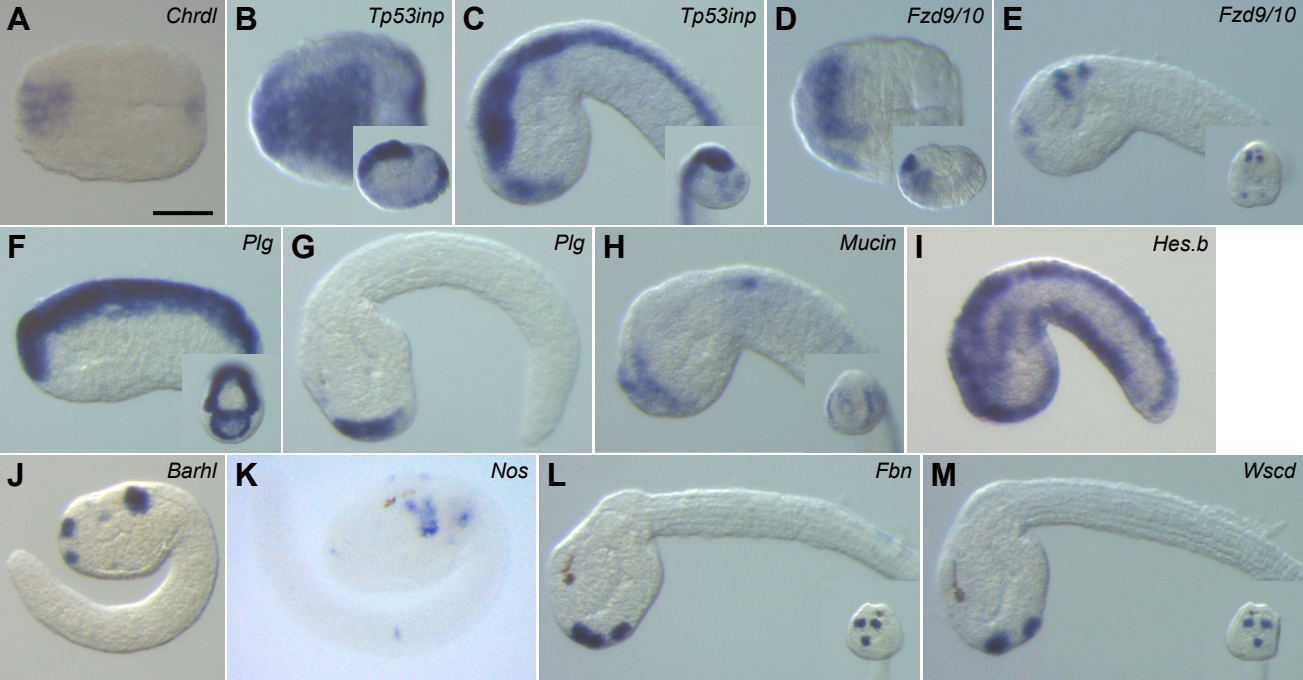
A
Chrdl
B
Tp53inp
C
Tp53inp
D
Fzd9/10
E
Fzd9/10
F
Plg
G
Plg
H
Mucin
I
Hes.b
J
Barhl
K
Nos
L
Fbn
M
Wscd